6052 *Biochemistry* **2009,** *48,* 6052–6061
DOI: 10.1021/bi900154f

BIOCHEMISTRY
including biophysical chemistry & molecular biology
Article

Structure, Dynamics, and Activity of an All-Cysteine Mutated Human β Defensin-3 Peptide Analogue[†]

Karthik Balakrishna Chandrababu,[‡] Bow Ho,[§] and Daiwen Yang*[,∥]

[‡]*Department of Chemistry, 3 Science Drive 3, Faculty of Science, National University of Singapore, Singapore 117543,* [§]*Department of Microbiology, 5 Science Drive 2, Yong Loo Lin School of Medicine, National University of Singapore, Singapore 117597, and* [∥]*Department of Biological Sciences, 14 Science Drive 4, Faculty of Science, National University of Singapore, Singapore 117543*

Received January 30, 2009; Revised Manuscript Received May 29, 2009

ABSTRACT: Human β defensin-3 (HBD-3) is a unique potent antimicrobial peptide. To explore the importance of the three-dimensional structure of HBD-3 in its activity and selectivity, we have mutated all six cysteine residues of HBD-3 to other amino acids, expressed the mutant (named as Def-A) in *Escherichia coli*, and analyzed the mutant's activity, structure, and dynamics. Def-A is active against several bacterial strains, but the activity is influenced by the ionic strength of the environment. When subjected to vesicles like POPG or to micelles like SDS, Def-A is changed from a random coil structure to an ordered helical form. We have determined the structure of Def-A in SDS micelle and found that it is folded into two distinct helices separated by a proline kink. We propose that the long N-terminal helix with many hydrophobic residues is inserted inside the micelle while the C-terminal helix with one large positive charge patch is located outside the micelle and interacts with the charged head groups of the micelle. The model is supported by NMR relaxation and H−D exchange data. Our results indicate that in addition to the number of positively charged residues and hydrophobic residues, the arrangement of these residues in the three-dimensional space is important to the antimicrobial selectivity and salt-dependent activity of human β defensins.

The ability of the innate immune system to recognize and neutralize microbial invaders shows the efficacy of the host defense settings for any living being. This innate immune system actually remains as a physical barrier by producing deterrents known as antimicrobial peptides (AMPs)[1] to prevent the entry of invading microorganisms. Defensins comprise a large family of AMPs and are classified into three different subfamilies (α, β, and θ defensins). Most of them are cationic, small, and amphiphilic with fewer than 50 amino acids showing activity against a vast number of deadly microorganisms like bacteria, fungi, and enveloped viruses. Human β defensins belong to the subfamily of β defensins. These peptides are known to contain both cationic and hydrophobic residues which are considered to be the prerequisite for their ability to disrupt bacterial membranes (*1*). It has been reported previously that the number and distribution of positively charged residues and hydrophobic residues play a major role in the activity and cytotoxicity for any antimicrobial peptides (*2*). However, the underlying principle of their action mechanism is still under study for the development of their analogues as therapeutic drugs.

Among all the human defensins, human β defensin-3 (HBD-3) is known to exhibit many interesting features such as an unusually high positive charge (+11), a broad spectrum of activity, and relative insensitivity to low salt concentrations (*3*). It also has low lytic activity on the human erythrocytes and shows no cytotoxic effect against human cells (*3*). Along with HBD-3, the three-dimensional structures of a number of other defensins have been determined by NMR and X-ray spectroscopy (*4*−*8*). Several investigations show that HBD-3 is active against *Escherichia coli*, *Pseudomonas aeruginosa*, *Klebsiella pneumonia*, *Staphylococcus aureus*, *Streptococcus pyogenes*, *Enterococcus faecium*, *Streptococcus pneumoniae*, *Staphylococcus carnosus*, and many others (*3*, *9*−*13*). Even though HBD-3 is highly potent against many strains, some strains like *Burkholderia* are known to be highly resistant to HBD-3 (*14*). This shows that HBD-3 is not only potent but also relatively selective. Previous studies demonstrate that the membrane-induced helix in HBD-3 might be important for its selection of bacterial membranes (*15*). On the other hand, the activity and cytotoxicity of HBD-3 depend on its overall positive charge distribution and hydrophobicity. When the natural HBD-3 was isolated originally, its disulfide connectivity was not determined, and it was presumed to belong to the β defensin family (*3*). For various β defensins, including HBD-3, the presence and position of S−S bonds and N-terminal sequence variations seem to have only a marginal effect on their activities

[†]This work was supported by the National University of Singapore.
*To whom correspondence should be addressed. Telephone: 65-6516-1014. Fax: 65-6779-2486. E-mail: dbsydw@nus.edu.sg.
[1]Abbreviations: AMP, antimicrobial peptide; HBD-3, human β defensin-3; IPTG, isopropyl β-D-thiogalactopyranoside; POPG, 1-palmitoyl-2-oleoyl-*sn*-glycero-3-[phospho-*rac*-(1-glycerol)] (sodium salt); SDS, sodium dodecyl sulfate; NMR, nuclear magnetic resonance; TFA, trifluoroacetic acid; CD, circular dichroism; NOE, nuclear Overhauser effect; MIC, minimum inhibitory concentration; MHB, Mueller−Hinton broth; LUV, large unilamellar vesicles.

 Published on Web 05/29/2009

at low concentrations of NaCl (<25 mM) or divalent ions like Ca^{2+} and Mg^{2+} (<0.1 mM) (*2*, *10*, *16*−*18*), but only wild-type HBD-3 with correct disulfide bridges is relatively insensitive up to 150 mM of NaCl when tested for *S. aureus* (*3*). In contrast to the antimicrobial effect, the chemotactic-mediated activity is clearly susceptible to changes in S−S arrangement (*10*). A recent report shows that through careful mutations it is possible to separate the chemotactic and antimicrobial activities of HBD-3 even when it is devoid of any S−S linkages (*13*). The activity of HBD-3 is confined with its lipid specificity, and thus, HBD-3 is more selective against certain strains and safe for mammalian cells (*19*). Although there are many findings on various aspects of HBD-3 (*20*), the structure−activity relationship still remains largely unknown.

In this study, we examined the activity of a HBD-3 analogue with all Cys residues replaced with other residues and found it active against different strains but only at low ionic strengths. We also determined the structure and dynamics of the analogue in SDS micelles. Different from the native HBD-3 that forms a short helical segment followed by a three-stranded antiparallel sheet in aqueous solution, the analogue adopts a random coil structure in water and folds into two distinct helices separated by a proline kink in the SDS micelle environment. The results indicate that the antimicrobial activity and selectivity of human β defensins are determined by not only the numbers of positively charged and hydrophobic residues but also the three-dimensional (3D) structure.

MATERIALS AND METHODS

Expression and Purification of Def-A and Reduced HBD-3. The amino acid sequences (Figure 1A) of reduced HBD-3 (rHBD-3) and its analogue, Def-A, were back-translated to obtain the DNA sequence. Two synthetic primers of 88 and 98 bases (Sigma-Proligo) overlapped for synthesis of the desired gene sequence. For Def-A, the forward primer is an 88-mer (5′-GATCATGGCACATATGGGTATTATTAATACTCTGCA-GAAATATTATGCGCGTGTGCGTGGTGGTCGTTACG-CGGTGCTGAGCGTGCTG-3′) containing the start codon (ATG) together with the NdeI cutting site in the 5′ region just before the peptide sequence and a 21 bp overlap in the 3′ region of a 98-mer reverse primer. Similarly, the reverse primer (5′-ATCCGCTCGAGCTACTTCTTGCGGCGCACCTTCTTG-CGGCCGCGAGTGCTCACCTTGCCGATCTGCTCCTCC-TTCGGCAGCACGCTCAGCACCGCGTA-3′) has a stop codon before the XhoI cutting site in the 5′ region and a 21 bp overlapping region at its 3′ end. Similar forward and reverse primers were designed for the rHBD-3 peptide with codons to generate all six Cys residues at their original positions. The codons were all optimized for overexpression in the *E. coli* BL21 (DE3) strain. The polymerase chain reaction (PCR) was used to construct the synthetic gene. The PCR mixture consisted of 0.4 unit of Advantage 2 Taq polymerase (Clontech), 0.5 μL of each primer at 10 mM, 2 μL of 10 mM dNTPs, 6 μL of $MgCl_2$, and 10 μL of 10 × PCR buffer in a total volume of 100 μL. The PCR conditions were as follows: one cycle at 94 °C for 30 s, 25 cycles at 94 °C for 30 s, 60 °C for 30 s, and 72 °C for 12 s, and a final extension at 72 °C for 10 min. The PCR product was cloned into a pET-32a-derived vector (devoid of the thioredoxin tag and the S tag) which was digested previously with the same restriction enzymes (NdeI and XhoI). The fidelity of the ligation product was confirmed by sequencing before it was introduced into the *E. coli* BL21(DE3) strain. A fresh clone of *E. coli* harboring the vector with the insert was grown in 5 mL of Luria-Bertani (LB) medium (containing 100 μg/mL ampicillin) overnight at 37 °C and then diluted into 1 L of M9 minimal medium with 1 g of $^{15}NH_4Cl$ to continue culturing at the same temperature until the midlog phase (OD_{600} = 0.6). The cells were then incubated using 0.2 mM IPTG (isopropyl β-D-thiogalactopyranoside) for 14 h at 16 °C before being harvested. Harvested cells were lysed using ultrasonication in 10 mM phosphate buffer at pH 6.2. The peptide from the cell debris was extracted using 60% acetic acid and loaded directly into the RP-HPLC system with a C18 column for purification. Water with 0.1% TFA was used as running buffer A, and a gradient of acetonitrile with 0.1% TFA was used as buffer B for elution of the peptide. At 36% eluent B, the desired peptide was eluted at homogeneity and was checked using 16.5% tricine PAGE for purity, and its molecular weight was confirmed by ESI-MS.

Antibacterial Assay. The activity of Def-A and rHBD-3 was tested against two Gram-positive bacteria, *Bacillus megaterium IAM* 13418 T and *S. aureus* ATCC 25923, and two Gram-negative bacteria, *E. coli* ATCC 25922 and *P. aeuroginosa* ATCC 27853, using Hancock's microdilution assay for determining the MIC values (*21*). Briefly, bacteria were grown overnight (∼16 h) at 37 °C in 5 mL of Mueller−Hinton broth (MHB) to produce a bacterial concentration of 1×10^8 colony forming units (CFU)/mL (confirmed using colony count) and diluted in either quarter- or full-strength MHB to obtain a population of $\sim1\times10^6$ CFU/mL for testing with the peptides. The peptides were prepared in either full- or quarter-strength MHB medium in 2-fold serial dilutions from 200 to 6.25 μg/mL. For *B. megaterium*, the peptide concentrations were reduced further to determine the MIC. An aliquot of 50 μL of the peptide solution was added with 50 μL of the bacterial solutions into several microtubes, taking into consideration the fact that there is a 2-fold dilution in both of their final concentrations. The microtubes were shaken at 220 rpm for 16 h at 37 °C, and the MIC was determined as the lowest peptide concentration under which there is no visible growth of the tested isolates. Further colony count was done to confirm the population of the cells in selected tubes before and after the assay to validate the result. The assay was conducted in duplicate and repeated twice.

Preparation of Lipid Vesicles. Large unilamellar vesicles (LUV) of POPG (Avanti Polar Lipids, Alabaster, AL) were prepared by the previously described extrusion method (*22*, *23*). Briefly, the chloroform in the POPG lipid mixture was evaporated to dryness using a stream of N_2 gas and further subjected to vacuum overnight. Dry lipid film was resuspended in phosphate buffer (pH 7.4) to hydrate them to form multilamellar vesicles. The lipid suspension was frozen and thawed several times using liquid N_2 and hot water and then extruded 20 times through polycarbonate membranes with 100 nm diameter pores to generate homogeneous LUV.

CD Spectroscopy. The secondary conformational properties of Def-A in different buffers were recorded in a Jasco J810 spectropolarimeter (Jasco Corp., Tokyo, Japan) at room temperature using 0.1 cm path length cuvettes. All samples were prepared in a 10 mM sodium phosphate buffer (pH 7.4) for recording the spectra in micelles (SDS) and vesicles (POPG). The peptide concentration was maintained at 20 μM in all cases, and the concentrations of both SDS and POPG vesicles were maintained well above their individual critical micelle concentration (CMC) (20 mM for SDS and 1 mM for POPG).

Isothermal Titration Calorimetry. ITC experiments were performed at 25 °C on a Microcal VP-ITC machine. The cell and syringe were filled with solutions of 50 μM Def-A and 0.5 mM POPG LUV, respectively. Both samples were prepared using 10 mM phosphate buffer (pH 7.4) and degassed for 10 min prior to being used. To measure the heat change upon binding, the titrant was introduced into the cell through 30 injections of 10 μL aliquots at an interval of 4 min. The duration of each injection was set at 20 s, and the contents of the reaction cell were stirred continuously at 300 rpm. The heat of dilution was adjusted by subtracting the heat produced during a control experiment in which POPG LUV were titrated into the phosphate buffer containing no peptide. The thermodynamic parameters were obtained by fitting the ITC data using a single-site binding model provided with Origin 5. Further ΔG and ΔS were calculated using the relations $\Delta G = -RT \ln K_a$ and $\Delta S = (\Delta H - \Delta G)/T$, respectively.

NMR Spectroscopy. All NMR spectra were recorded at 35 °C on a Bruker Avance 500 MHz spectrometer equipped with a cryoprobe. The sample was prepared in 500 μL of H_2O containing 0.5 mM peptide, 5% D_2O, and 50 mM SDS-d_{25} micelles. The pH of the final solution was adjusted to 4.2 using diluted NaOH and HCl. Three-dimensional (3D) ^{15}N-edted TOCSY-HSQC and 3D ^{15}N-edited NOESY-HSQC spectra were recorded for resonance assignment and structure determination; 512 complex points were recorded at a spectral width (SW) of 8012 Hz for the direct observation ^{1}H dimension, and 128 complex points were recorded at a SW of 4502 Hz for the indirect ^{1}H dimension. For ^{15}N, a total of 44 complex points were recorded at a SW of 1115 Hz. All experiments were conducted using a relaxation delay of 1 s. The ^{15}N time domain data were doubled by linear prediction. The data were zero-filled and Fourier-transformed to obtain a final data set comprising 1024, 128, and 256 data points in the direct ^{1}H dimension and indirect ^{15}N and ^{1}H dimensions, respectively. The raw data were processed using NMRPipe (*24*), and resonance assignments were made using the NMR package and Sparky (*25*). Backbone and side chain ^{1}H and ^{15}N spins were assigned from the two 3D spectra, and all the NOEs were obtained from two-dimensional (2D) and 3D NOESY spectra recorded with mixing times of 80 and 100 ms, respectively.

Relaxation Study. ^{15}N relaxation experiments were conducted using the same sample as the one used for the structural studies. Relaxation times T_1 and $T_{1\rho}$ and $\{^1H\}-^{15}N$ heteronuclear NOEs were measured using the inversely detected 2D NMR experiments as described previously (*26*, *27*). T_1 relaxation times were measured by recording a series of 2D spectra at the following time delays: 10, 100, 200, 360, 440, 550, and 650 ms. A recycle delay of 1 s and eight scans were used. $T_{1\rho}$ values were measured using relaxation delays of 5, 40, 60, 80, 100, and 130 ms at a spin-lock power of 1.6 kHz, a recycle delay of 2.5, and eight scans. $\{^1H\}-^{15}N$ NOE data were obtained from the signal intensities measured with and without ^{1}H saturation. For proton saturation, a train of 120° ^{1}H pulses was applied for a period of 3 s after a recycle delay of 3 s. Each spectrum with spectral widths of 912 Hz for ^{15}N and 8012 Hz for ^{1}H was recorded using 100 and 512 complex points in t_1 and t_2 dimensions, respectively.

Structure Calculation. The distance restraints were generated from $^1H-^1H$ NOE cross-peak intensities obtained from the NOESY spectra after calibration. Initial structures were generated by backbone torsion angle restraints and distance geometry using CYANA-2.1 (*28*). A total of 200 structures were calculated, and 10 lowest-energy structures with no distance violations

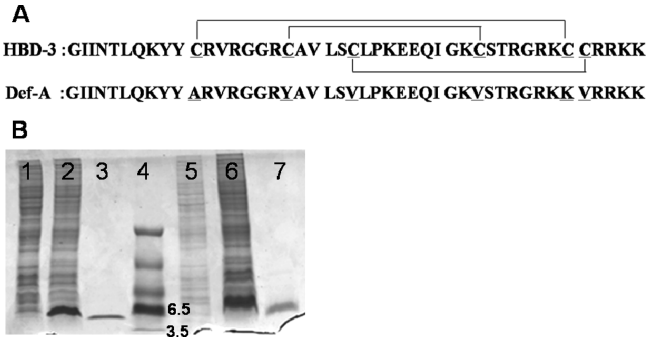

FIGURE 1: Sequence comparison of Def-A with HBD-3 and Tricine PAGE of Def-A and rHBD-3. (A) The primary amino acid sequences of both HBD-3 and Def-A were aligned to show the cysteine mutations. The disulfide pattern in HBD-3 is shown using straight lines, and cysteine and mutated residues are underlined where rHBD-3 is devoid of any disulfide linkages. (B) A 16.5% Tricine gel shows the expression level and purified bands of Def-A and rHBD-3: lanes 1−3, results before induction, results after induction, and purified fractions of Def-A, respectively; lane 4, molecular marker; and lanes 5−7, results before induction, results after induction, and purified fractions of rHBD-3, respectively.

greater than 0.2 Å or dihedral angle violations larger than 2° were selected for further refinement using CYANA's built-in simulated annealing protocol.

Relaxation Data Analysis. Spin−spin relaxation time T_2 was calculated using the following equation

$$1/T_{1\rho} = 1/T_1 \sin^2\theta + 1/T_2 \cos^2\theta \quad (1)$$

where $\theta = \text{atan}(\Delta\omega/\omega_1)$, in which $\Delta\omega$ is the resonance offset and ω_1 is the spin-lock field strength. The relaxation data were analyzed using the following relations (*29*):

$$1/T_1 = d^2/4[3J(\omega_N) + J(\omega_H - \omega_N) + 6J(\omega_H + \omega_N)] + c^2 J(\omega_N) \quad (2)$$

$$1/T_2 = d^2/8[4J(0) + 3J(\omega_N) + J(\omega_H - \omega_N) + 6J(\omega_H) + 6J(\omega_H + \omega_N)] + c^2/6[4J(0) + 3J(\omega_N)] \quad (3)$$

$$\text{NOE} = 1 + T_1(\gamma^H/\gamma^N)(d^2/4)[6J(\omega_H + \omega_N) - J(\omega_H - \omega_N)] \quad (4)$$

where $d = (\mu_0 h/8\pi^2)\gamma^H\gamma^N r_{NH}^{-3}$, $c = \omega_N(\sigma_\parallel - \sigma_\perp)/\sqrt{3}$,$\gamma$ is the gyromagnetic ratio, h is Planck's constant, μ_0 is the permeability of vacuum, r_{NH} is the N−H bond length (1.02 Å), and $\sigma_\parallel$ and $\sigma_\perp$ are the parallel and perpendicular components, respectively, of the assumed axial symmetric chemical shift tensor ($\sigma_\parallel - \sigma_\perp$ = 170 ppm). A single overall tumbling time is insufficient for describing the overall motion of a nonspherical or unfolded protein. To obtain physically meaningful order parameters for Def-A that is partially unfolded, we used our previously established method (*30*, *31*) to extract dynamics parameters on a per residue basis. In this case, the spectral density function $J(\omega)$ is given by

$$J(\omega) = 0.4[S^2\tau_{loc}/(1 + \omega^2\tau_{loc}^2) + (1 - S^2)\tau_e/(1 + \omega^2\tau_e^2)] \quad (5)$$

where τ_{loc} is the apparent correlation time for a specific residue and τ_e is the effective correlation time that satisfies the relation $\tau_e \ll \tau_{loc}$.

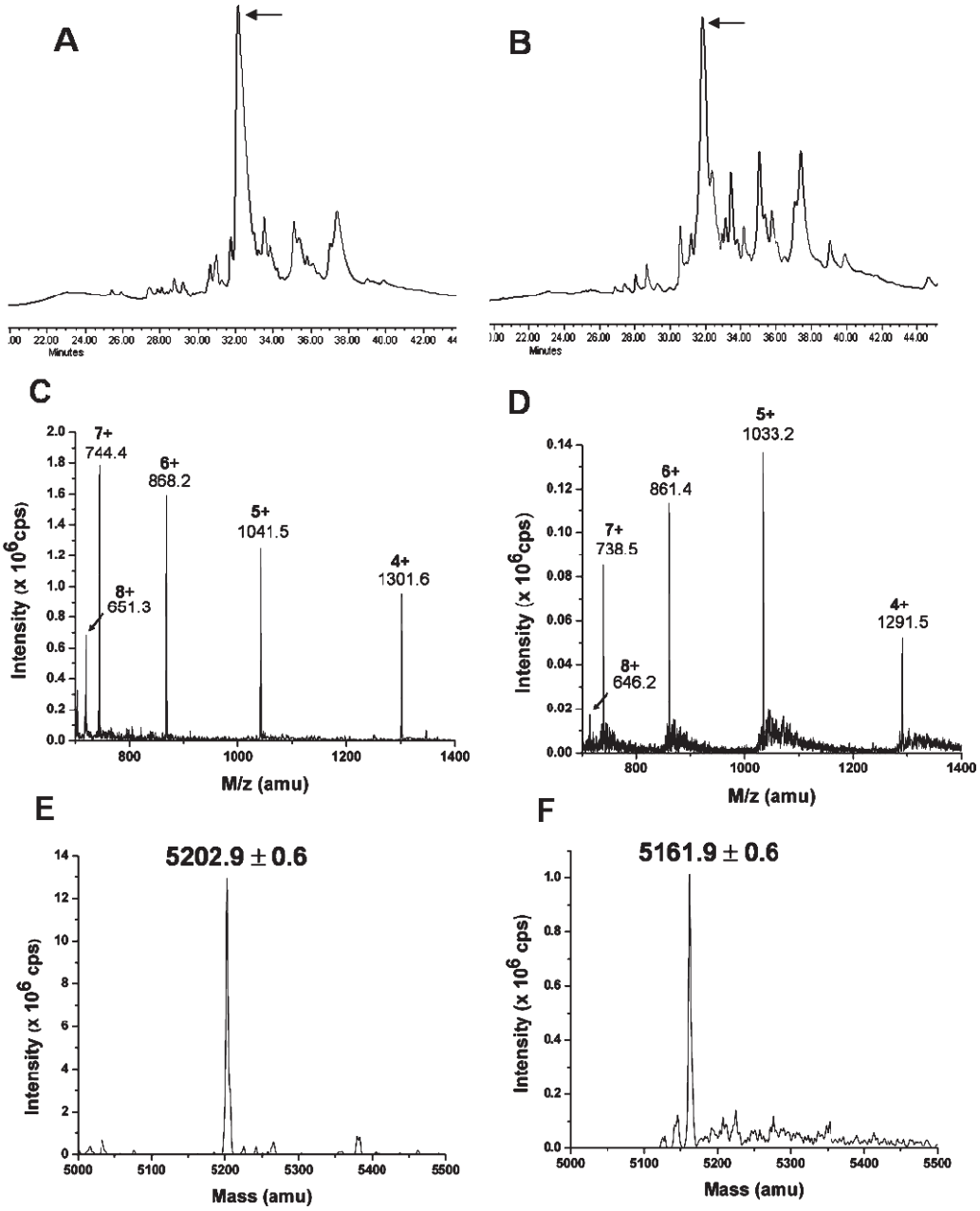

FIGURE 2: Analytical HPLC profiles and ESI-MS determination. (A and B) Elution profiles of Def-A and rHBD-3 when loaded into a Waters C-18 analytical column and eluted using an acetonitrile gradient. Arrowheads indicate the peaks of Def-A and rHBD-3. (C and D) ESI-MS analysis of unlabeled Def-A and rHBD-3, respectively, with a series of multiple charged ions corresponding to the homogeneous peptides. (E and F) Molecular masses of unlabeled Def-A (5202.9 ± 0.6 Da) and rHBD-3 (5161.9 ± 0.6 Da).

Table 1: Minimum Inhibitory Concentrations[a] (MIC in micrograms per milliliter) for Def-A and rHBD-3 Peptides against Gram-Positive and Gram-Negative Bacteria

peptide	*B. megaterium* IAM 13418T	*S. aureus* ATCC 25923	*E. coli* ATCC 25922	*P. aeuroginosa* ATCC 27853
Def-A	3.13	12.5	12.5	12.5
rHBD-3	3.13	25.0	25.0	25.0

[a] The assay was conducted using a quarter-strength of Mueller−Hinton broth.

RESULTS AND DISCUSSION

Design and Preparation of Def-A. The linear analogue of HBD-3 (Figure 1A) was designed to study the importance of the 3D structure in its activity. All the cysteine residues were mutated with an intension to examine the influence of the peptide conformation on the activity and its binding to different membrane mimicking reagents. The linear peptide was designed so that there is a slight increase in the overall hydrophobicity and positive charge. The first Cys was mutated to Ala to facilitate the α-helical formation in the N-terminal region similar to the short helix seen in the wild type. The second to last Cys was changed to a basic residue to increase the overall charge, while others were chosen to slightly increase the hydrophobicity. HBD-3 in its completely reduced form was also expressed to compare its activity with that of Def-A. The expression conditions were optimized such that both the peptides could be extracted directly from the inclusion body after ultrasonication. During sonication, most of the impurities were solubilized in the lysis buffer. The acetic acid extract was further purified with RP-HPLC, and pure

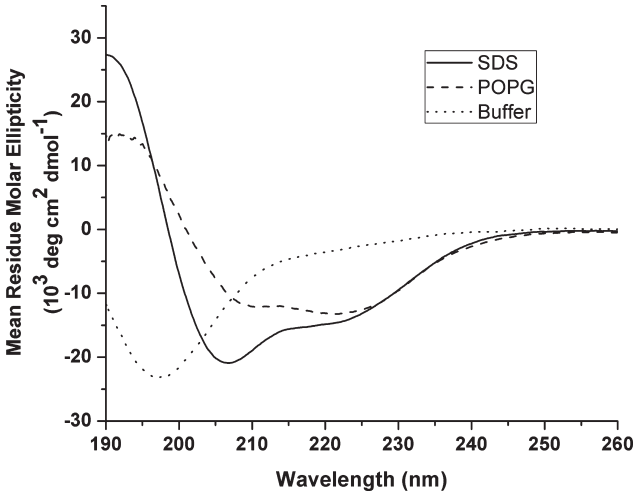

FIGURE 3: Circular dichroism spectra of Def-A under different conditions. The far-UV CD spectra of 20 μM Def-A recorded in 10 mM phosphate buffer (···), 20 mM micelles of SDS (—), and 1 mM POPG vesicles (---).

Table 2: Thermodynamic Parameters of Interaction of Def-A with POPG Vesicles

K_a ($\times 10^6$ M^{-1})	17.54 ± 3.86
ΔH (kcal mol^{-1})	−8.564 ± 0.072
ΔS (cal K^{-1} mol^{-1})	4.435
ΔG (kcal mol^{-1})	−9.871
K_d ($\times 10^{-9}$ M)	57.01

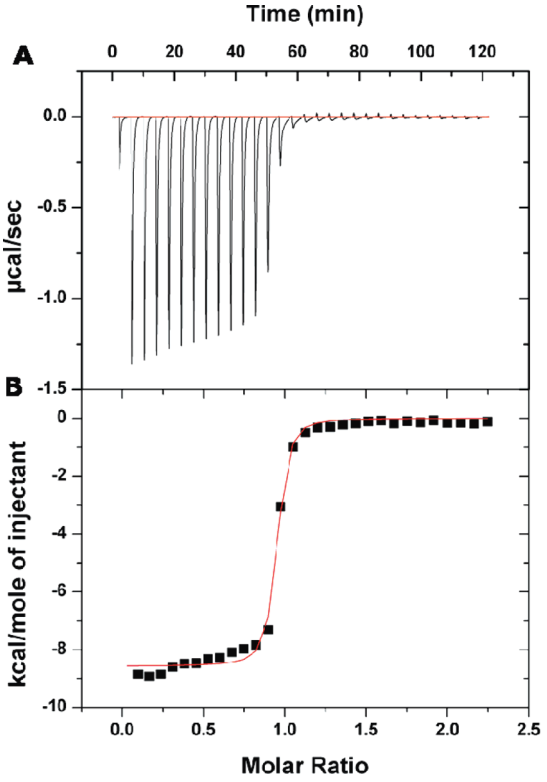

FIGURE 4: Isothermal calorimetric titrations for the binding of Def-A to POPG vesicles. (A) Injection of 10 μL aliquots containing 0.5 mM POPG vesicles into a solution of 50 μM Def-A in 10 mM phosphate buffer (pH 7.4) resulting in the spikes, reflecting the heat change upon each addition. (B) Plots of the heat change as a function of POPG:Def-A molar ratio.

peptides were obtained (Figures 1B and 2A,B). Because of the slight increase in hydrophobicity, Def-A was eluted with a 1 min delay under identical conditions (Figure 2A,B). Overall, this new method has reduced the number of purification steps and facilitated the purification procedure. A final yield of ~8 mg of protein/L of culture was obtained. The lyophilized sample had very high solubility in pure water because of its high dielectric constant. rHBD-3 was expressed in a completely reduced form under our experimental conditions, and special care was taken to maintain its reduced form throughout the experiments. The lyophilized rHBD-3 was dissolved in water and treated with 100 mM DTT for 1 h to make sure that there are no S−S bonds present, and the mixture was again purified by HPLC. The eluted rHBD-3 was lyophilized and purged with N_2 gas to remove the air contaminants and aliquoted into several tubes and stored at −80 °C until it was needed. The reduced state of rHBD-3 was confirmed using ESI-MS before and after the experiment (Figure 2D,F).

Activity against Bacterial Strains. To test the activity of Def-A and rHBD-3 on two Gram-positive (*B. megaterium* and *S. aureus*) and two Gram-negative (*E. coli and P. aeuroginosa*) bacterial strains, we used Hancock's microdilution method. The MIC value, which is defined as the minimum concentration of the peptide required to inhibit the visible growth of bacteria, was determined using this method. The results (Table 1) were highly consistent for all the repeats. Except for *B. megaterium* (the activity against this strain is not available for wild-type HBD-3 in the literature), wild-type HBD-3 is more active than its analogues against all the strains used here as shown previously (*3*, *9*−*13*). Here we find that both our peptides were active only at low ionic strengths (containing 0.13 mM Ca^{2+} and 0.10 mM Mg^{2+}) which is quite comparable with the results published by other groups (*2*, *9*), while Def-A shows slightly higher activity than rHBD-3. This can be explained on the basis of the increased hydrophobicity and positive charge of Def-A due to mutation. At a higher ionic strength (0.5 mM Ca^{2+} and 0.4 mM Mg^{2+}), there is a considerable decrease in activity (MIC ≥ 300 μg/mL for both the peptides) which is different from the wild type's specific salt insensitive behavior (*3*). Previously, many researchers have clearly shown that the presence of cations in the medium will affect the electrostatic interaction of the mutant peptides with the negatively charged bacterial cell wall, but either very high hydrophobicity or oligomerization level might overcome this effect (*2*). Hence, we conducted the study of amphipathic structure in the presence of model mimicking agents to explore further the reason behind this kind of behavior.

Conformational Change upon Binding to Model Membranes. Both SDS and POPG molecules share similar negatively charged headgroups and aliphatic tail regions. SDS can form micelles, while POPG can form vesicles. Thus, they can be used to mimic bacterial membranes. Def-A changed its secondary structure from a random coil form to an α-helix structure when subjected to any membrane-mimicking medium as seen from the CD spectra (Figure 3). The secondary structure of Def-A in POPG vesicles is different from that in SDS (Figure 3), indicating that even though both membrane models share a similar charge at the headgroup the peptide conformation is different due to the size, length, and arrangement of the molecules forming the micelle or vesicle. This explains the influence of the environment on the peptide conformation.

Isothermal Titration Calorimetry. The strong affinity for POPG or SDS is an indirect indication of the efficiency and

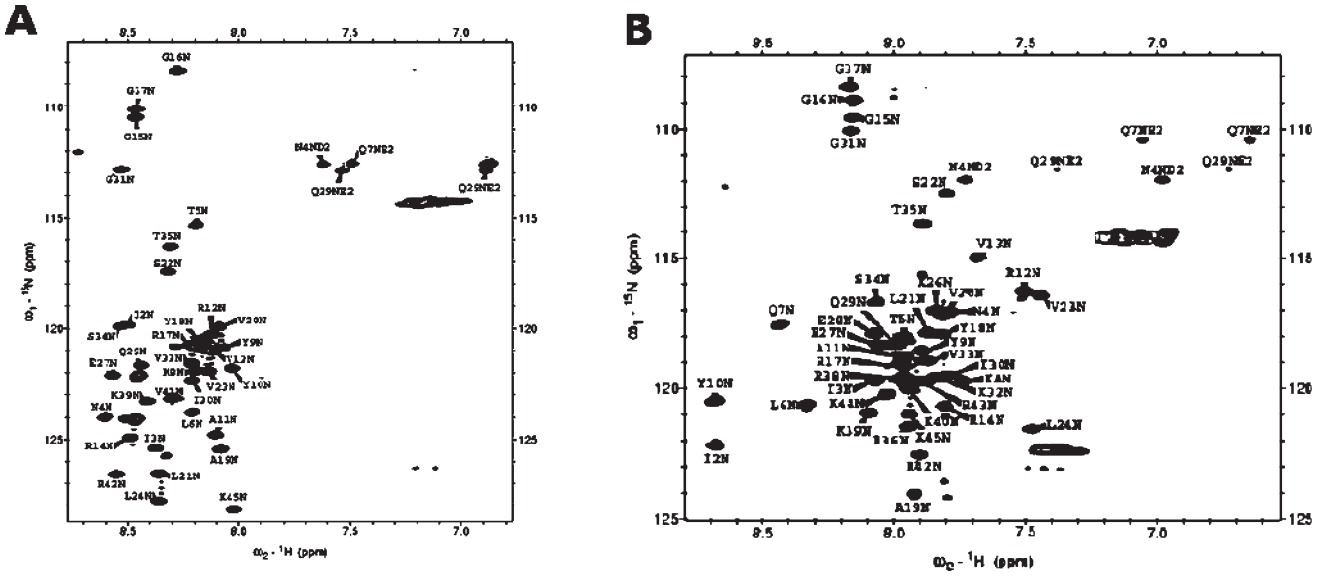

FIGURE 5: ^{1}H−^{15}N heteronuclear single-quantum correlation spectra of 0.5 mM Def-A (A) in water at 15 °C and (B) in 50 mM SDS micelles at 35 °C.

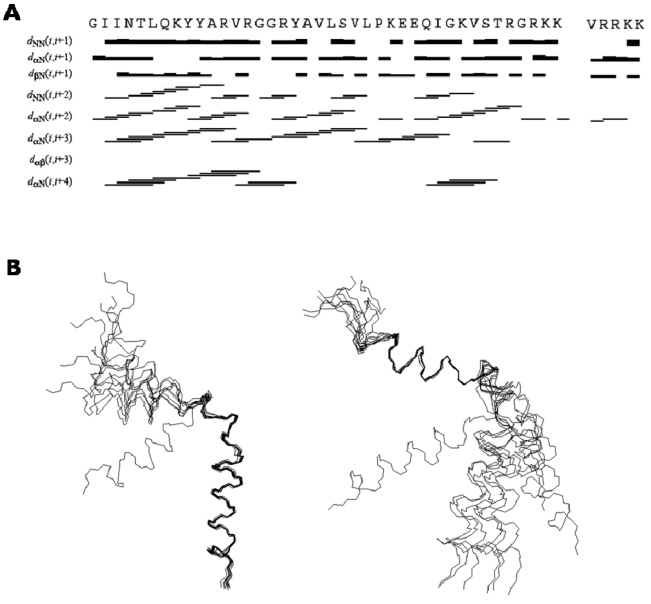

FIGURE 6: NOE intensities and connectivities and the solution structure of SDS-bound Def-A. (A) Relative intensities and connectivities of NOEs and (B) superposition of 10 lowest-energy structures for SDS-bound Def-A: (left) superposition of residues 1−27 and (right) superposition of residues 27−38. The structures were generated using Molmol (*35*).

potency of an AMP. The enthalpy change upon Def-A binding to the negatively charged POPG vesicles was hence investigated in isothermal calorimetric experiments. The heat change upon addition of POPG was saturated after 15 injections (~60 min), indicating the completion of the binding process. Figure 4A shows the binding thermogram and Figure 4B the dependence of the net heat of binding on the POPG:Def-A molar ratio. The ITC titration profile clearly shows that the binding between Def-A and POPG is exothermic. The thermodynamic parameters (Table 2) determined from the experiment indicate that the binding is entropically driven with nanomolar affinity. Determining the structure of Def-A bound to POPG vesicles would be comparatively more suitable than Def-A bound to SDS micelles, but the large size of the vesicle made it unsuitable for NMR studies.

Table 3: NMR and Structure Statistics for the SDS-Bound Peptide

total no. of NOE restraints	496
intraresidue	174
sequential ($\|i-j\| = 1$)	228
medium-range ($1 < \|i-j\| < 5$)	94
long-range	0
dihedral angle restraints	52
hydrogen bond restraints	0
structure statistics	
no. of distance violations of > 0.20 Å	2
no. of dihedral angle violations of > 5°	0
maximum dihedral angle violation (deg)	3.89
maximum distance constraint violation (Å)	0.37
average root-mean-square deviation (Å)	
backbone atoms (full-length)	2.420
backbone atoms (residues 1−27)	0.393
backbone atoms (residues 27−38)	0.166

NMR Studies of Def-A in the SDS-Bound State. The one-dimensional (1D) ^{1}H spectrum of Def-A in the absence of SDS shows that Def-A adopts a random coil structure in water, while the 1D ^{1}H spectrum in the presence of 50 mM SDS indicates that Def-A forms certain structures in micelles, consistent with the CD data (Figure S1 of the Supporting Information). Panels A and B of Figure 5 show the 2D ^{15}N−^{1}H HSQC spectra with assignments for Def-A in the absence and presence of SDS, respectively. All peaks in the presence of SDS are broader than those in the absence of SDS due to the binding of Def-A to SDS micelles. We observed very few NOEs in aqueous solution which were insufficient to define the structure of free Def-A. Hence, we determined only the structure for the SDS-bound form (Table 3). Resonance assignments were made according to the methods published previously (*32*, *33*). We assigned ~90% NOE peaks in the 3D ^{15}N-edited NOESY-HSQC spectrum and obtained 496 unambiguous NOEs.

The relative NOE intensities and connectivities are shown in Figure 6A. The characteristic $d_{\alpha N}(i, i+4)$ NOEs, which can generally be observed for α-helices, were present in the segments of I2−Y18 and Q29−T35, although the chemical shift index (derived from Ha only) shows the entire peptide has a strong propensity to form helical structures except for several residues (Figure S2 of the Supporting Information). The absence of $d_{\alpha N}$

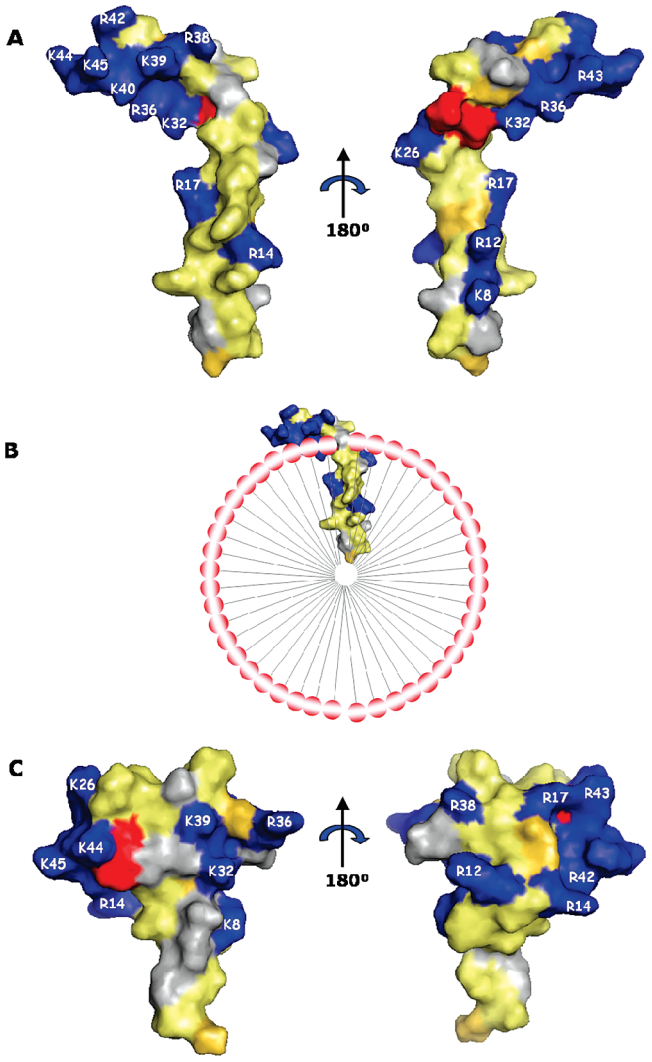

FIGURE 7: Surface of Def-A and HBD-3. (A) Surface representations of Def-A showing the charge and hydrophobic clusters and patches. Positive charge patch 1 consisted of K8, R12, and R17; patch 2 consisted of K32, R36, R38, K39, K40, R42, R43, K44, and K45. (B) Model showing the insertion of Def-A into the SDS micelle. The headgroups of all SDS molecules are shown as spheres with red tinge and their aliphatic tail regions as straight lines. The diameter of the SDS micelle is ~50 Å, and the length of the helical segment inside the micelle is ~27 Å. (C) Surface representations of HBD-3 (Protein Data Bank entry 1kj6) showing two positive charge patches. Patch 1 consists of R14, R17, K26, R42, R43, K44, and K45; patch 2 consists of K32, K36, R38, and K39. The surfaces were generated using Pymol (http://pymol.sourceforge.net/), and the following colors were used for representing the residue types: blue for positively charged residues (K and R), pale yellow for hydrophobic residues (A, I, L, Y, and V), red for negatively charged residues (E), and gray for others (N, Q, S, and T).

$(i, i+4)$ and $d_{NN}(i, i+2)$ in the C-terminal region indicates that this region is devoid of any helical structure. A total of 496 NOE restraints (174 intraresidue, 228 sequential, and 94 medium-range) and 52 dihedral angle restraints derived from chemical shifts with TALOS (*34*) were used for structure calculation. The refined structure of Def-A shows two helices (one long and the other short) separated by a proline residue at the 25th position (which introduces a kink between them) and no interactions between the two helices (Figure 6B). The N-terminal long helix is composed of more hydrophobic residues than the C-terminal helix. The presence of a few charged residues in the first long helix weakens its interaction with the hydrophobic core of the SDS micelles.

The surface diagram (Figure 7A) of Def-A shows clearly that the positively charged residues cluster in the C-terminal segment and the hydrophobic residues cluster in its long N-terminal segment. The root-mean-square deviations for N-terminal (Gly-1−Glu-27) and C-terminal (Glu-27−Arg-38) segments were 0.39 and 0.17 Å, respectively. Because there were no observable NOE restraints between the two segments, their relative positioning was quite poorly determined. Nevertheless, it is clear that the second helix bends toward the first one because of the presence of P25. Interestingly, the hydrophobic residues are distributed on one face of each helix, while charged residues are on the other face. This distribution can enhance the interaction of the peptide with the micelle or with the bacterial membrane. The N-terminal helix is 27 Å long, and this helix can comfortably fit into the interior of the SDS micelle which is 40−50 Å in diameter (*36*−*38*). Therefore, we propose that the first helix is located inside the micelle and interacts with the micelle tails through hydrophobic interactions, while the second helix is partially exposed to the outside of the micelle and interacts with the micelle headgroups through charge−charge interactions (Figure 7B). This model is further supported by the amide H−D exchange data; i.e., residues I3, L6, Y9, Y10, A11, R12, R14, L21, V23, and L24 in the long helix had very slow H−D exchange rates ($< 2 \times 10^{-5}$ s^{-1}), while all residues in the second helix had much higher H−D exchange rates. We could not exclude the possibility of the positively charged N-terminus of the peptide being outside the micelle, but the second and third residues (I2 and I3) should be inside to interact with the hydrophobic tail of SDS since they are hydrophobic and the amide proton of I3 is protected from exchange with solvent deuterons.

Previous studies of the reshuffling of disulfide bonds or mutation of the cysteine residues of HBD-3 have revealed the following. (a) Upon being subjected to SDS micelles, the wild type and any of its linear analogues show increases in helical content (*18*, *39*). (b) Neither reduction nor interchange of disulfide bonds has a significant effect on the activity of HBD-3 (*10*). (c) Linear analogues in which all cysteines are substituted with hydrophobic residues like Trp or Phe show activity comparable to that of the wild type, but if the residues are substituted with Ala or Tyr, the activity is decreased (*2*, *18*). (d) Only the number and proper distribution of positively charged residues and hydrophobic residues determine the potency of the peptides (*2*). Further, it has been shown that the specificity of HBD-3 is altered by mutations, and the derivatives lose their preferential inhibition and become significantly more salt sensitive (*2*). These results imply that detailed structural studies are important for understanding the mechanisms of HBD-3 and its analogues against microbes.

Although the 3D structure of wild-type HBD-3 in the presence of SDS (or membrane mimics) is not available, the overall structure of the monomeric form should not be affected by SDS because the three pairs of disulfide bonds restrict conformational changes. A previous study using CD has demonstrated that the percentage of the β-conformation of HBD-3 remains unaltered, though the α-helical content increases in the presence of SDS micelles (the N-terminal α-helix could be longer in SDS) (*39*). Therefore, the HBD-3 structure in the absence of SDS can be approximated as the overall structural fold of HBD-3 in the presence of SDS. A structural comparison

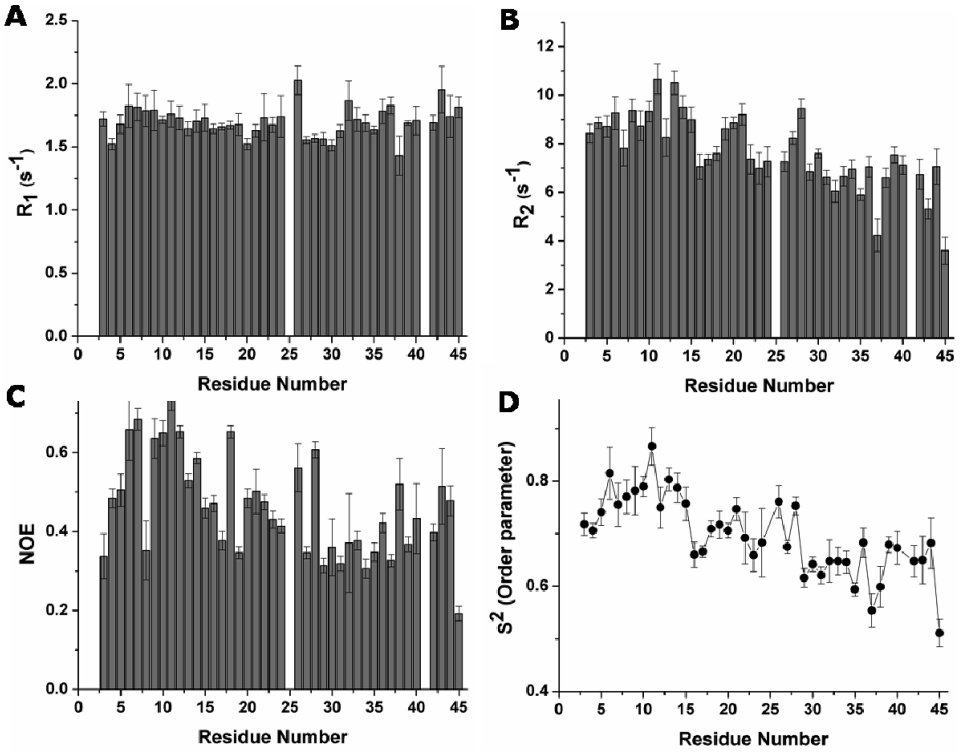

FIGURE 8: Relaxation data and order parameters of SDS-bound Def-A. The longitudinal relaxation rate R_1 (A), transverse relaxation rate R_2 (B), $\{^1H\}-^{15}N$ heteronuclear NOE (C), and order parameter (D) are plotted vs residue number.

of HBD-3 and SDS-bound Def-A shows that both have positively charged residues asymmetrically distributed between their hydrophobic patches (Figure 7A,C). The presence of disulfide linkages in HBD-3 leads to a more compact structure with one small and one large positively charged patch (patch 1, R14, R17, K26, R42, R43, K44, and K45; patch 2, K32, K36, R38, and K39). The charged patches are separated by one large hydrophobic patch. The residues in Def-A also form one small and one large positively charged patch (patch 1, K8, R12, and R17; patch 2, K32, R36, R38, K39, K40, R42, R43, K44, and K45). However, the two charge patches are located in two noninteracting helices. In addition, the hydrophobic patch is narrow and long for Def-A, rather than wide as for HBD-3. Since Def-A contains more hydrophobic and charged residues than HBD-3, it is indeed more potent than the reduced rHBD-3, but it is less potent than wild-type HBD-3 (with disulfide bonds) against most bacterial strains at the same ionic strength. Thus, the significant difference in the distribution of charged residues and hydrophobic residues over the 3D structures can be attributed to the differences in the activity and specificity of HBD-3 and Def-A. In addition, Def-A exists in a monomeric form since no intermolecular NOEs were observed. On the other hand, wild-type HBD-3 may exist in a dimeric form because of its unique 3D structure (*6*). The dimeric form has a significantly higher positive net charge than the monomeric analogues. This may explain why the wild type is significantly less sensitive to salt concentration than its analogues in antimicrobial activity.

According to our model (Figure 7B), mutations of nonhydrophobic residues in the first helix of a linear HBD-3 analogue to hydrophobic residues will enhance peptide−micelle (membrane) interactions and thus increase the activity of the peptide. This explains why the Cys to Ala and Tyr mutants have significantly lower activity than the Cys to Trp and Phe mutants (*2*, *18*).

Relaxation Parameters of Def-A. To determine the backbone dynamics of SDS-bound Def-A, we measured ^{15}N relaxation rates R_1 and R_2 along with the $\{^1H\}-^{15}N$ NOE (Figure 8A−C). In the first helical segment (Ile-3−Leu-24), the average R_2 and NOE values were 8.58 ± 1.04 s^{-1} and 0.52 ± 0.12, respectively, while in the second helix (Glu-27−Arg-38), they were 6.84 ± 1.27 s^{-1} and 0.38 ± 0.09, respectively. On the other hand, R_1 values were quite uniform over the entire sequence. The average order parameters for the first and second helices were 0.74 ± 0.05 and 0.64 ± 0.05, respectively, showing that the long helix is more rigid than the short one. The backbone flexibility indicates that the long helix is more restricted than the shorter one in motion, consistent with our model; i.e., the long helix is embedded inside the micelle, while the short helix is partially exposed to the outside.

CONCLUSION

Def-A, a HBD-3 analogue, contains no cysteine residues and has a 3D structure very different from that of HBD-3. Like many linear antimicrobial peptides, Def-A adopts a random coil conformation in aqueous solution and forms helical structures in membrane-mimicking media. Def-A may target bacteria by approaching the cell surface through the electrostatic interaction and then further disrupting the membrane with the insertion of the long helix into the cell membrane wall. Although Def-A contains more positively charged residues and hydrophobic residues than HBD-3, it is active only at low ionic strength and hence should differ from the HBD-3's mechanism of antimicrobial action. This indicates the significance of the 3D structural differences between Def-A and HBD-3 in its antimicrobial activity. Further, understanding the interaction of wild-type HBD-3 with the cell membrane or membrane mimics will provide more insights into the structure−activity relationship.

ACKNOWLEDGMENT

We are grateful to Prof. R. M. Kini for providing the ESI-MS facility, Prof. T. Wohland in the Department of Chemistry for assistance in POPG LUV preparation, and Mr. H. C. Ng in the Department of Microbiology for assistance in antibacterial assay experiment.

SUPPORTING INFORMATION AVAILABLE

One figure showing the 1D ^{1}H spectra of Def-A in the presence and absence of SDS and one figure showing the chemical shift index of Def-A in the presence of SDS. This material is available free of charge via the Internet at http://pubs.acs.org.

REFERENCES

(1) Ganz, T., and Lehrer, R. I. (1994) Defensins. *Curr. Opin. Immunol. 6*, 584–589.
(2) Kluver, E., Schulz-Maronde, S., Scheid, S., Meyer, B., Forssmann, W. G., and Adermann, K. (2005) Structure-activity relation of human β-defensin 3: Influence of disulfide bonds and cysteine substitution on antimicrobial activity and cytotoxicity. *Biochemistry 44*, 9804–9816.
(3) Harder, J., Bartels, J., Christophers, E., and Schroder, J. M. (2001) Isolation and characterization of human β-defensin-3, a novel human inducible peptide antibiotic. *J. Biol. Chem. 276*, 5707–5713.
(4) Hoover, D. M., Chertov, O., and Lubkowski, J. (2001) The structure of human β-defensin-1: New insights into structural properties of β-defensins. *J. Biol. Chem. 276*, 39021–39026.
(5) Hoover, D. M., Rajashankar, K. R., Blumenthal, R., Puri, A., Oppenheim, J. J., Chertov, O., and Lubkowski, J. (2000) The structure of human β-defensin-2 shows evidence of higher order oligomerization. *J. Biol. Chem. 275*, 32911–32918.
(6) Schibli, D. J., Hunter, H. N., Aseyev, V., Starner, T. D., Wiencek, J. M., McCray, P. B. Jr., Tack, B. F., and Vogel, H. J. (2002) The solution structures of the human β-defensins lead to a better understanding of the potent bactericidal activity of HBD3 against *Staphylococcus aureus*. *J. Biol. Chem. 277*, 8279–8289.
(7) Hill, C. P., Yee, J., Selsted, M. E., and Eisenberg, D. (1991) Crystal structure of defensin HNP-3, an amphiphilic dimer: Mechanisms of membrane permeabilization. *Science 251*, 1481–1485.
(8) Szyk, A., Wu, Z., Tucker, K., Yang, D., Lu, W., and Lubkowski, J. (2006) Crystal structures of human α-defensins HNP4, HD5, and HD6. *Protein Sci. 15*, 2749–2760.
(9) Hoover, D. M., Wu, Z., Tucker, K., Lu, W., and Lubkowski, J. (2003) Antimicrobial characterization of human β-defensin 3 derivatives. *Antimicrob. Agents Chemother. 47*, 2804–2809.
(10) Wu, Z., Hoover, D. M., Yang, D., Boulegue, C., Santamaria, F., Oppenheim, J. J., Lubkowski, J., and Lu, W. (2003) Engineering disulfide bridges to dissect antimicrobial and chemotactic activities of human β-defensin 3. *Proc. Natl. Acad. Sci. U.S.A. 100*, 8880–8885.
(11) Shelburne, C. E., Coulter, W. A., Olguin, D., Lantz, M. S., and Lopatin, D. E. (2005) Induction of β-defensin resistance in the oral anaerobe *Porphyromonas gingivalis*. *Antimicrob. Agents Chemother. 49*, 183–187.
(12) Starner, T. D., Agerberth, B., Gudmundsson, G. H., and McCray, P. B. Jr. (2005) Expression and activity of β-defensins and LL-37 in the developing human lung. *J. Immunol. 174*, 1608–1615.
(13) Taylor, K., Clarke, D. J., McCullough, B., Chin, W., Soe, E., Yang, D., Oppenheim, J., Uhrin, D., Govan, J. R., Campopiano, D. J., Macmillan, D., Barran, P., and Dorin, J. R. (2008) Analysis and separation of residues important for the chemoattractant and antimicrobial activities of β defensin 3. *J. Biol. Chem. 283*, 6631–6639.
(14) Sahly, H., Schubert, S., Harder, J., Rautenberg, P., Ullmann U., Schroder, J., and Podschun, R. (2003) *Burkholderia* is highly resistant to human β-defensin 3. *Antimicrob. Agents Chemother. 47*, 1739–1741.
(15) Morgera, F., Antcheva, N., Pacor, S., Quaroni, L., Berti, F., Vaccari, L., and Tossi, A. (2008) Structuring and interactions of human β-defensins 2 and 3 with model membranes. *J. Pept. Sci. 14*, 518–523.
(16) Mandal, M., Jagannadham, M. V., and Nagaraj, R. (2002) Antibacterial activities and conformations of bovine β-defensin BNBD-12 and analogs: Structural and disulfide bridge requirements for activity. *Peptides 23*, 413–418.
(17) Krishnakumari, V., Sharadadevi, A., Singh, S., and Nagaraj, R. (2003) Single disulfide and linear analogues corresponding to the carboxy-terminal segment of bovine β-defensin-2: Effects of introducing the β-hairpin nucleating sequence D-Pro-Gly on antibacterial activity and biophysical properties. *Biochemistry 42*, 9307–9315.
(18) Liu, S., Zhou, L., Li, J., Suresh, A., Verma, C., Foo, Y. H., Yap, E. P., Tan, D. T., and Beuerman, R. W. (2008) Linear analogues of human β-defensin 3: Concepts for design of antimicrobial peptides with reduced cytotoxicity to mammalian cells. *ChemBioChem 9*, 964–973.
(19) Böhling, A., Hagge, S. O., Roes, S., Podschun, R., Sahly, H., Harder, J., Schröder, J. M., Grötzinger, J., Seydel, U., and Gutsmann, T. (2006) Lipid-specific membrane activity of human β-defensin-3. *Biochemistry 45*, 5663–5670.
(20) Dhople, V., Krukemeyer, A., and Ramamoorthy, A. (2006) The human β-defensin-3, an antibacterial peptide with multiple biological functions. *Biochim. Biophys. Acta 1758*, 1499–1512.
(21) Wiegand, I., Hilpert, K., and Hancock, R. E. (2008) Agar and broth dilution methods to determine the minimal inhibitory concentration (MIC) of antimicrobial substances. *Nat. Protoc. 3*, 163–175.
(22) Prenner, E. J., Lewis, R. N., Kondejewski, L. H., Hodges, R. S., and McElhaney, R. N. (1999) Differential scanning calorimetric study of the effect of the antimicrobial peptide gramicidin S on the thermotropic phase behavior of phosphatidylcholine, phosphatidylethanolamine and phosphatidylglycerol lipid bilayer membranes. *Biochim. Biophys. Acta 1417*, 211–213.
(23) Jing, W., Hunter, H. N., Hagel, J., and Vogel, H. J. (2003) The structure of the antimicrobial peptide Ac-RRWWRF-NH_2 bound to micelles and its interactions with phospholipid bilayers. *J. Pept. Res. 61*, 219–229.
(24) Delaglio, F., Grzesiek, S., Vuister, G. W., Zhu, G., Pfeifer, J., and Bax, A. (1995) NMRPipe: A multidimensional spectral processing system based on UNIX pipes. *J. Biomol. NMR. 6*, 277–293.
(25) Goddard, T. D., and Kneller, D. G. (2003) Sparky 3 , University of California, San Francisco.
(26) Farrow, N. A., Zhang, O., Forman-Kay, J. D., and Kay, L. E. (1995) Comparison of the backbone dynamics of a folded and an unfolded SH3 domain existing in equilibrium in aqueous buffer. *Biochemistry 34*, 868–878.
(27) Mikael, A., and Arthur, G. P. (1996) Monitoring Macromolecular Motions on Microsecond to Millisecond Time Scales by $R_{1\rho}$-R_1 Constant Relaxation Time NMR Spectroscopy. *J. Am. Chem. Soc. 118*, 911–912.
(28) Herrmann, T., Guntert, P., and Wuthrich, K. (2002) Protein NMR structure determination with automated NOE assignment using the new software CANDID and the torsion angle dynamics algorithm DYANA. *J. Mol. Biol. 319*, 209–227.
(29) Farrow, N. A., Zhang, O., Szabo, A., Torchia, D. A., and Kay, L. E. (1995) Spectral density function mapping using ^{15}N relaxation data exclusively. *J. Biomol. NMR. 6*, 153–162.
(30) Yang, D., Mok, Y. K., Forman-Kay, J. D., Farrow, N. A., and Kay, L. E. (1997) Contributions to protein entropy and heat capacity from bond vector motions measured by NMR spin relaxation. *J. Mol. Biol. 272*, 790–804.
(31) Ran, X., Miao, H., Sheu, F. S., and Yang, D. (2003) Structural and dynamic characterization of a neuron-specific protein kinase C substrate, neurogranin. *Biochemistry 42*, 5143–5150.
(32) Marion, D., Driscoll, P. C., Kay, L. E., Wingfield, P. T., Bax, A., Gronenborn, A. M., and Clore, G. M. (1989) Overcoming the overlap problem in the assignment of ^{1}H NMR spectra of large proteins by use of three-dimensional heteronuclear ^{1}H-^{15}N Hartmann-Hahn-multiple quantum coherence and nuclear Overhauser-multiple quantum coherence spectroscopy: Application to interleukin 1β. *Biochemistry 28*, 6150–6156.
(33) Wuthrich, K. (1986) NMR of Proteins and Nucleic Acids , John Wiley, New York.
(34) Cornilescu, G., Delaglio, F., and Bax, A. (1999) Protein backbone angle restraints from searching a database for chemical shift and sequence homology. *J. Biomol. NMR 13*, 289–302.
(35) Koradi, R., Billeter, M., and Wuthrich, K. (1996) MOLMOL: A program for display and analysis of macromolecular structures. *J. Mol. Graphics 14*, 51–55.

(36) Hayter, J. B., and Penfold, J. (1981) Self-consistent structural and dynamic study of concentrated micelle solutions. *J. Chem. Soc., Faraday Trans. 77*, 1851–1863.
(37) Sheu, E. Y., Wu, C. F., Chen, S. H., and Blum, L. (1985) Application of a rescaled mean spherical approximation to strongly interacting ionic micellar solutions. *Phys. Rev. A 32*, 3807–3810.
(38) Itri, R., and Amaral, L. Q. (1991) Distance distribution function of sodium dodecyl sulfate micelles by X-ray scattering. *J. Phys. Chem. 95*, 423–427.
(39) Boniotto, M., Antcheva, N., Zelezetsky, I., Tossi, A., Palumbo, V., Verga Falzacappa, M. V., Sgubin, S., Braida, L., Amoroso, A., and Crovella, S. (2003) A study of host defence peptide β-defensin 3 in primates. *Biochem. J. 374*, 707–714.